Hybridization of Peptide Nucleic Acid†

Tommi Ratilainen,‡ Anders Holmén,*,‡ Eimer Tuite,‡ Gerald Haaima,§ Leif Christensen,§ Peter E. Nielsen,§ and Bengt Nordén‡

Department of Physical Chemistry, Chalmers University of Technology, S-412 96 Gothenburg, Sweden, and Center for Biomolecular Recognition, The Panum Institute, Department of Biochemistry B, Blegdamsvej 3c, DK-2200 N Copenhagen, Denmark

Received April 17, 1998; Revised Manuscript Received June 24, 1998

ABSTRACT: The thermodynamics of hybridization and the conformations of decameric mixed purine-pyrimidine sequence PNA/PNA, PNA/DNA, and DNA/DNA duplexes have been studied using fluorescence energy transfer (FET), absorption hypochromicity (ABS), isothermal titration calorimetry (ITC), and circular dichroism (CD) techniques. The interchromophoric distances determined in the FET experiments on fluorescein- and rhodamine-labeled duplexes indicate that the solution structures of the duplexes are extended helices in agreement with available NMR (PNA/DNA) and crystal X-ray data (PNA/PNA). The melting thermodynamics of the duplexes was studied with both FET and ABS. The thermodynamic parameters obtained with ABS are in good agreement with the parameters from calorimetric measurements while FET detection of duplex melting gives in most cases more favorable free energies of hybridization. This discrepancy between FET and ABS detection is ascribed to the conjugated dyes which affect the stability of the duplexes substantially. Especially, the dianionic fluorescein attached via a flexible linker either to PNA or to DNA seems to be involved in an attractive interaction with the opposite dicationic lysine when hybridized to a PNA strand. This interaction leads to an increased thermal stability as manifested as a 3−4 °C increase of the melting temperature. For the PNA/DNA duplex where fluorescein is attached to the PNA strand, a large destabilization ($\Delta T_m = -12$ °C) occurs relative to the unlabeled duplex, probably originating from electrostatic repulsion between the fluorescein and the negatively charged DNA backbone. In the case of the PNA/PNA duplex, the sense of helicity of the duplex is reversed upon conjugation of fluorescein via a flexible linker arm, but not when the fluorescein is attached without a linker to the PNA.

Oligonucleotides and their mimics are becoming increasingly interesting for use as gene-targeted drugs and molecular biology tools (*1*, *2*). Among these, peptide nucleic acids (PNAs) have been shown to have certain advantages compared to other analogues (*3*, *4*). In PNA, the negatively charged backbone of DNA is completely exchanged for a neutral achiral pseudopeptide, composed of *N*-(2-aminoethyl)glycine units, onto which the nucleobases are attached (Figure 1).

A mixed-sequence PNA strand can hybridize with complementary single-stranded DNA, RNA, or another PNA strand to form stable duplexes with high sequence-selectivity (*3*−*5*). The thermal stabilities increase in the series DNA/DNA < PNA/DNA < PNA/PNA (*5*, *6*). According to NMR experiments, PNA/DNA mixed-sequence duplexes adopt a structure possessing features of both A-form and B-form DNA (*7*), while oligopyrimidine PNAs with homopurine polynucleotides form triplex structures analogous to DNA triplexes, as concluded from flow linear dichroism and CD (*8*). The PNA/PNA duplex was inferred to be a B-DNA-like helical complex from CD measurements (*9*). However, X-ray diffraction studies have shown that a PNA/PNA duplex in a crystal adopts a unique P-form helix structure with

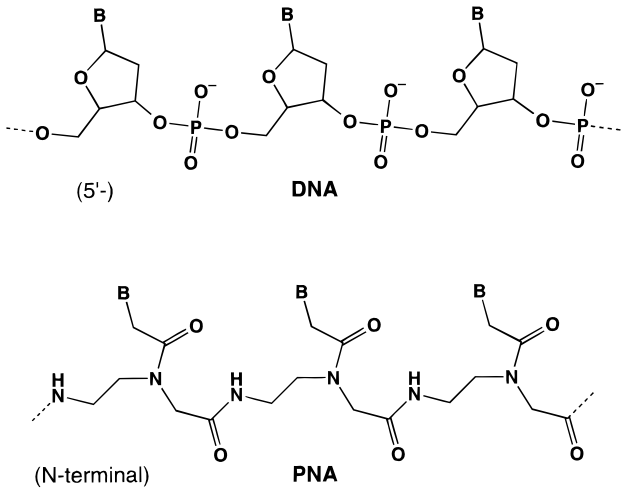

FIGURE 1: Chemical structures of DNA and PNA. The deoxyribose phosphate ester backbone in DNA has been changed to *N*-(2-aminoethyl)glycine in PNA.

† Financial support from the Swedish Cancer Foundation (B.N.), the EU Biomed 2 Program (BMH4-CT96-0848, B.N.), and the Danish National Research Foundation (P.E.N.) is gratefully acknowledged. E.T. and A.H. thank the EU TMR program (ERBCHBGCT940548) and the Chemistry Division at Chalmers University of Technology, respectively, for research fellowships.

* To whom correspondence should be addressed. E-mail: holmen@phc.chalmers.se. Phone: +46-31-772 30 49. Fax: +46-31-772 38 58.

‡ Chalmers University of Technology.

§ The Panum Institute.

S0006-2960(98)00872-1 CCC: $15.00
Published on Web 08/14/1998

perpendicularly stacked bases, and with a helical rise of 18 base pairs per turn and a diameter of 28 Å (*10*). Recent molecular modeling and molecular dynamics simulation studies gave solution structures for the PNA/PNA and PNA/DNA duplexes in good agreement with the aforementioned experimental data (*11*). It has also been observed that polypyrimidine PNAs can displace the homopyrimidine strand of a duplex homopurine-homopyrimidine target to form a triplex on the purine target (*3*).

PNAs might find applications as anti-sense reagents, as artificial suppressors of gene expression (*12, 13*), or as activators of transcription (*14*). In the field of biotechnology, PNA oligomers have been found useful in many of the applications in which traditional synthetic oligonucleotides are used, however, with the additional benefits of having a higher binding affinity to nucleic acid targets and resistance to nuclease and proteolytic degradation. Applications include restriction enzyme blocking (*15*), screening for genetic mutations (*16*), and nucleic acid capture enhancement of the selectivity of PCR (*17*).

Fluorescent probes and FET have been widely used in the DNA field, to detect hybridization (*18, 19*), and to study the thermodynamics and kinetics of hybridization (*20*). Using FET, overall distance and structural information about nucleic acids has been obtained (*21, 22*).

We here report on FET, absorption hypochromicity (ABS), circular dichroism (CD), and isothermal titration calorimetry (ITC) measurements made in order to characterize structural and thermodynamic aspects of the interactions of the PNA/DNA duplex binding motif and to compare it with PNA/PNA and DNA/DNA duplexes. Important issues are to distinguish the relative importance of enthalpic and entropic contributions to the free energy of hybridization, whether the hybridization can be described by a two-state equilibrium model, or if any significant precursor outer-sphere complexes are formed (which FET would reveal sensitively). Finally, we investigate using FET if the somewhat hydrophobic character of PNA might lead to folded or collapsed structures in solution.

MATERIALS AND METHODS

Chemicals. Two mixed-sequence complementary decamers of PNA (*23*) and DNA were studied; base sequences and notations are given in Figure 2. The fluorescent dyes were end-conjugated to the PNAs via a linker consisting of an aminohexanoic acid (-aha-) and a thiourea group, formed when fluorescein isothiocyanate (Molecular Probes, Eugene) or tetramethylrhodamine isothiocyanate (Fluka) are reacted with the amino end of the aminohexanoic acid (Figure 2). For fluorescein attached to the oligonucleotide, the linker was 6-amino-2-hydroxymethyl-1-hexanol (-ahh-), and the rhodamine-labeled oligonucleotide was obtained from MedProbe AS, Oslo, with the same linker (-ahh-). As references for determinations of extinction coefficients of the dyes, we used fluorescein and tetramethylrhodamine isothiocyanates, respectively, conjugated to the methyl ester of glycine.

All experiments were carried out in 10 mM sodium phosphate buffer (pH 7.7), except for the quantum yield reference which was fluorescein in 0.1 M NaOH.

Absorption Measurements. Absorption spectra were recorded on a Cary 4 spectrophotometer. Concentration determinations of the unlabeled strands were based on absorption at 260 nm measured at 80 °C. At 80 °C, the nucleobases are considered completely destacked, and the absorptivity is therefore assumed to be the sum of the absorptivities of DNA monomers taken from literature (*24*). For the studied sequences, one obtains an effective $\epsilon_{260} = 112 \times 10^3$ cm^{-1} M^{-1} per single strand. The absorptivity determinations of the labels were accomplished by comparing the absorptivity profiles of the fluorescently labeled PNA strands and those of the free labels (attached to a glycine), all measured at 80 °C. Setting the ϵ_{max} value of the residual, i.e., the contribution of the nucleobases, to the value found above, $\epsilon_{260} = 112 \times 10^3$ cm^{-1} M^{-1} at 80 °C, the fluorescein maximum absorptivity was calculated as $\epsilon_{500} = 81 \times 10^3$ cm^{-1} M^{-1} for the PNA-conjugated and $\epsilon_{496} = 64 \times 10^3$ cm^{-1} M^{-1} at 80 °C for the DNA-conjugated fluorescein, both at 80 °C. The corresponding procedure for rhodamine gave $\epsilon_{556} = 91 \times 10^3$ cm^{-1} M^{-1} for both PNA- and DNA-conjugated rhodamine, using the ϵ_{260} value from above. Both these values are quite high and close to the literature values of the *free* fluorescein and rhodamine labels (*25*).

Hybridizations. The appropriate single strands were hybridized by the following procedure: heating of the solutions of single strands to 80 °C, adjustment of concentration (2−3 μM in strands) by absorbance measurements, mixing (at 80 °C) of the single-strand solutions, and slow-cooling to room temperature (20 °C). The samples of fluorescently labeled oligomers, used for the energy transfer experiments, are either duplexes of fluorescein-labeled oligomers hybridized to unlabeled complementaries (donor alone, D) or duplexes of fluorescein-labeled oligomers hybridized to rhodamine-labeled complementaries (donor in the presence of acceptor, DA), e.g., Fl-aha-PNA1/PNA2 (D) and Fl-aha-PNA1/PNA2-aha-Rh (DA). For the other duplexes studied, see Figure 2. The acceptor-labeled and the unlabeled strands were used in approximately 20% excess in the hybridizations, to minimize the possibility of having nonhybridized donors in the samples.

Fluorescence Energy Transfer. The rate of energy transfer from a specific donor to a specific acceptor, according to Förster's theory of fluorescence energy transfer (*26*−*28*), is given by

$$k_T = \frac{1}{\tau_D}\left(\frac{R_0}{R}\right)^6 \qquad (1)$$

where τ_D is the donor lifetime in absence of the acceptor, R_0 the critical Förster distance, and R the actual distance. The R_0 value is the distance at which the energy transfer accounts for half of the deactivation processes of the donor. It is calculated from

$$\left(\frac{R_0}{\text{cm}}\right)^6 = (8.79 \times 10^{-25})\kappa^2 n^{-4} \phi_D J_{DA} \qquad (2)$$

where κ^2 is the orientation factor, n the refractive index of the medium between donor and acceptor, ϕ_D the quantum yield of the donor, and J_{DA} the overlap integral. The orientation factor is defined as

$$\kappa^2 = (\cos\theta_{DA} - 3\cos\theta_D \cos\theta_A)^2 \qquad (3)$$

a)

H-GTAGATCACT-lys-NH_2 (PNA1)

H_2N-lys-CATCTAGTGA-H (PNA2)

5′-GTAGATCACT-3′ (DNA1)

3′-CATCTAGTGA-5′ (DNA2)

b)

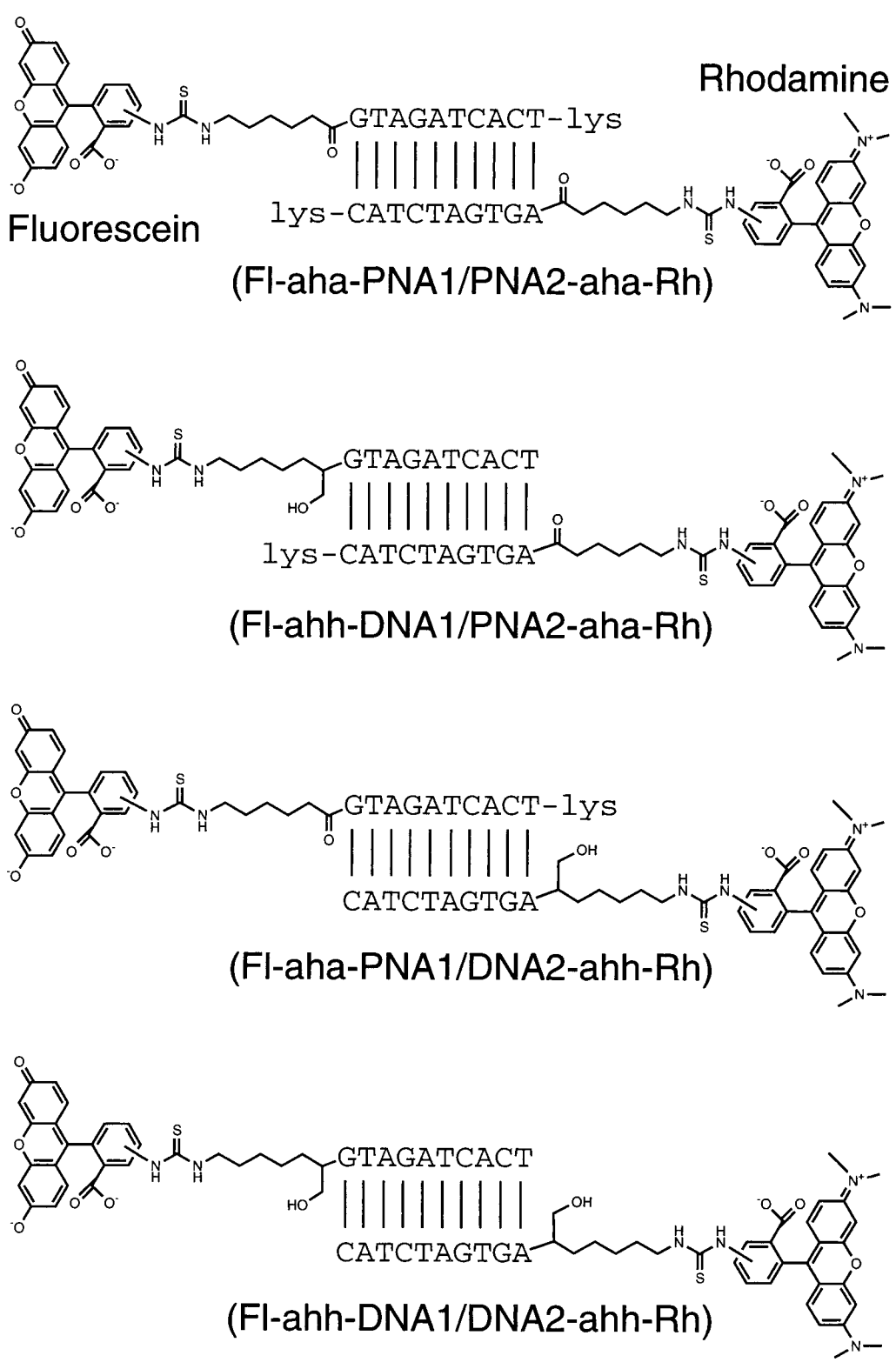

FIGURE 2: (a) Sequences of PNA and DNA used in this study (all lysines with L-configuration). (b) Schematic structures and notations of the fluorescently labeled PNAs and DNAs. Strands positioned in antiparallel orientation.

where the angles θ_{DA}, θ_A, and θ_D describe the relative orientations of the electric transition dipole moments (*29*). The overlap integral, J_{DA}, describes the spectral overlap between the emission spectrum of the donor and the absorption spectrum of the acceptor. It is defined as

$$J_{DA} = \frac{\int f_D(\lambda)\epsilon_A(\lambda)\lambda^4 \, d\lambda}{\int f_D(\lambda) \, d\lambda} \quad (4)$$

where $f_D(\lambda)$ is the corrected emission spectrum of the donor and $\epsilon_A(\lambda)$ the absorption spectrum of the acceptor.

The energy transfer efficiency, E, was calculated by comparing the fluorescence intensity, I_{DA}, of the donor in the donor/acceptor duplex with the intensity, I_D, of the donor strand in duplex with the complementary unlabeled strand.

$$E = 1 - \frac{I_{DA}}{I_D} \quad (5)$$

We also used the sensitized emission of the donor in order to determine E according to a method described by Clegg (*30*). Both approaches gave the same E within ±4% for all studied duplexes. Once the energy transfer efficiency and the critical Förster distance are determined, the actual distance, R, between the donor−acceptor pair can be calculated as

$$R = R_0\left(\frac{1}{E} - 1\right)^{1/6} \quad (6)$$

Circular dichroism (CD) is defined as the difference between the absorption of left, A_l, and right, A_r, circularly polarized light (*31*).

$$CD = A_l - A_r \quad (7)$$

CD measurements were made on a Jasco 700 spectropolarimeter. All CD spectra shown are noise-reduced by the algorithm in the software package, each spectrum checked "visually" not to be distorted.

Fluorescence measurements were performed on a SPEX Fluorolog τ2. The excitation wavelengths were chosen so as to excite the donor as selectively as possible (470 nm) or the acceptor only (560 nm). To check if any anisotropy might affect the fluorescence signals, measurements were performed both with and without polarizers at magic angle (*32*). This test showed no significant effect, and measurements were thereafter performed without the polarizers. In all measurements, the absorbance at the excitation wavelength was held sufficiently low (<0.05) to allow the inner-filter effect to be neglected (*33*). The spectral bandwidth was held constant at 1.8 nm in both the excitation and emission light paths. In all the temperature studies, the sample holder was held at a constant temperature using a thermostat-controlled water jacket. After each temperature change, the sample was equilibrated for approximately 3 min/(°C change).

The quantum yield of the fluorescein label, i.e., the donor, was determined from duplexes with the unlabeled complementary PNA sequence at different temperatures. The reference used was fluorescein in 0.1 M NaOH, with a quantum yield of 0.93 at room temperature (*34*). The same excitation wavelength, 470 nm, as for the energy transfer studies was used.

Fluorescence anisotropy (r) is a measure of the rotational mobility during the lifetime of the excited state of the fluorescent probes (*35*). It is defined as

$$r = \frac{I_{VV} - GI_{VH}}{I_{VV} + 2GI_{VH}} \quad (8)$$

where the first subscript refers to the excitation polarizer (V = vertical, H = horizontal) and the second one to the emission polarizer. $G = I_{HV}/I_{HH}$ is an instrumental correction factor.

Evaluation of Melting Curves. The physical property, i.e., absorbance at 260 nm or fluorescence energy transfer efficiency, plotted vs temperature, was fitted with a six-parameter function to a two-state model (*36*) of the hybridization. This model assumes that single strands are in equilibrium with only one base-paired duplex structure; i.e., there are no partially base-paired structures in the melting process (*37*). Furthermore, the change in heat capacity (ΔC_p°) between the two states is assumed to be zero, and the thermodynamic parameters ΔH° and ΔS° are assumed to be temperature-independent.

The equilibrium constant K can be expressed in either of the following exponential forms of eq 9 (depending on which pair of thermodynamic parameters are fitted: ΔH° and ΔS° or ΔH° and T_m) as well as in terms of the extent of reaction α (fraction of strands in duplex form):

$$K = e^{(-\Delta H^\circ/RT)+(\Delta S^\circ/R)} = \frac{4}{c_T/c^\circ} e^{(-\Delta H^\circ/R)[(1/T)-(1/T_m)]} = \frac{2\alpha}{(1-\alpha)^2 c_T/c^\circ} \quad (9)$$

c_T is the total concentration of single strands, and c° is the unit concentration 1 M. Solving for α gives an expression $\alpha = f(\Delta H^\circ, \Delta S^\circ, T)$ or $\alpha = g(\Delta H^\circ, T_m, T)$ which is combined with a model in which the physical property (e.g., A_{260} or E) of pure single- and double-stranded forms is allowed to vary with temperature according to a linear approximation: $A_s = m_s T + b_s$ and $A_d = m_d T + b_d$, yielding a fitting equation of the form

$$A = \alpha A_d + (1 - \alpha)A_s \quad (10)$$

containing a total of six fitting parameters: ΔH°, T_m, m_d, b_d, m_s, b_s (*37*−*39*). The deviations of m_s and m_d from zero can be regarded as a consideration of the temperature dependence of the intrinsic quantum yield and of nucleobase stacking dynamics.

Isothermal Titration Calorimetry (ITC). A MicroCal ITC MC-2 system was used in conjunction with an electronically controlled circulating water bath. A solution of one of the strands (about 5 μM) was placed in the cell (volume = 1.4 mL) and the titrant solution (about 0.1 mM) in a 100 μL syringe, whose needle is designed as a paddle-shaped stirrer rotating at 400 rpm. The syringe is controlled by a stepping motor, allowing precise injections (±0.1 μL). Typically 20 injections of 4 μL each and 5 min apart were made. The integrated peaks (pulses) of the heat production upon each injection were plotted against the molar ratio. With the

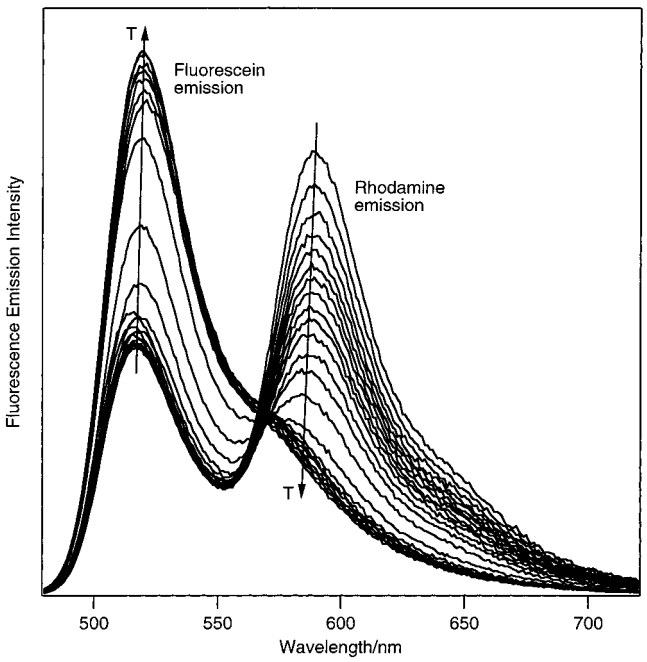

FIGURE 3: Fluorescence spectrum of the Fl-aha-DNA1/PNA2-aha-Rh complex as a function of temperature (1.5−87 °C). The sample was excited at 470 nm. The peaks at about 520 and 590 nm are characteristic of fluorescence from fluorescein and rhodamine, respectively.

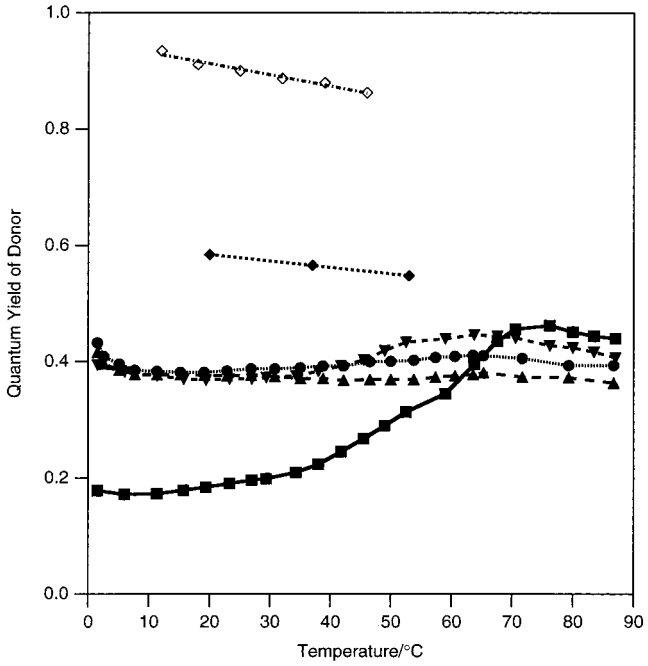

FIGURE 4: Quantum yields of fluorescein conjugated to PNA and DNA, respectively. Legend: (◇) free fluorescein, (◆) Fl-PNA1/PNA2, (■) Fl-aha-PNA1/PNA2, (▼) Fl-ahh-DNA1/PNA2, (●) Fl-aha-PNA1/DNA2, and (▲) Fl-ahh-DNA1/DNA2.

built-in software, MicroCal Origin, the binding isotherms were fitted to a two-state binding model, giving numerical values of both the enthalpy of binding (ΔH) and the binding constant (K).

RESULTS

Fluorescence Properties. In Figure 3 are shown representative fluorescence emission spectra of the Fl-aha-DNA1/PNA2-aha-Rh complex at various temperatures (1.5−87 °C). For the lower temperatures, the contributions from fluorescein and rhodamine emission at about 520 and 590 nm, respectively, are of comparable intensity, indicating extensive excitation energy transfer from fluorescein to rhodamine. At the excitation wavelength (470 nm), fluorescein absorbs about 90% of the exciting light and, thus, the contribution from directly excited rhodamine is almost negligible. That the rhodamine emission is due to energy transfer is also confirmed by the fluorescein-like excitation spectra measured at low temperature with the emission wavelength set to 650 nm where rhodamine fluorescence dominates (data not shown). With increasing temperature, the fluorescein emission intensity increases rapidly as the melting temperature is approached while that of rhodamine decreases; i.e., the energy transfer is switched off at the highest temperatures. This illustrates that the DNA/PNA duplex melts at the higher temperatures and the two strands separate, leading to distances between the fluorophores exceeding the critical transfer Förster distance (R_0) by several orders of magnitude.

To calculate R of eq 6, we first determine R_0, which involves determination of the donor fluorescence quantum yield, ϕ_D, and the overlap integral, J_{DA}, together with the orientation factor, κ^2. The temperature dependence of the donor (fluorescein) fluorescence quantum yield was determined for duplexes with one fluorescein-labeled PNA or DNA strand and one unlabeled PNA or DNA strand. The results for the Fl-PNA1/PNA2, Fl-aha-PNA1/PNA2, Fl-ahh-DNA1/PNA2, Fl-aha-PNA1/DNA2, and Fl-ahh-DNA1/DNA2 duplexes are displayed in Figure 4.

Also shown in Figure 4 is the temperature dependence of the fluorescence quantum yield of unconjugated fluorescein: with increasing temperature, the quantum yield decreases. By contrast, the quantum yields of all labeled duplexes, except for Fl-PNA1/PNA2, increase (or remain more or less constant) when going to higher temperatures (see below). Thus, it seems that fluorescein, attached to a flexible linker either on a PNA or on a DNA strand, is subject to a quenching process that is not as efficient at the elevated temperatures. The origin of this process will be discussed below. For Fl-PNA1/PNA2 which has the fluorescein attached directly to the PNA strand, the quantum yield decreases slightly with increasing temperature. The quantum yields of fluorescein conjugated to proteins and nucleic acids are between 0.2 and 0.5 at room temperature (*40*−*42*), so the values observed here (0.19−0.38) are as expected.

Values of the overlap integral (J_{DA}, eq 4) of Fl-aha-PNA1/PNA2-aha-Rh, Fl-ahh-DNA1/PNA2-aha-Rh, Fl-ahh-PNA1/DNA2-ahh-Rh, and Fl-ahh-DNA1/DNA2-ahh-Rh at different temperatures were determined using a maximum molar absorptivity of 91×10^3 cm^{-1} M^{-1} for rhodamine (see Materials and Methods). For Fl-aha-PNA1/PNA2-aha-Rh and Fl-ahh-PNA1/DNA2-ahh-Rh, J_{DA} was approximately constant, and equal to $(4.1 \pm 0.1) \times 10^{-13}$ cm^6 mmol^{-1}, over the entire temperature range, whereas for Fl-ahh-DNA1/PNA2-aha-Rh and Fl-ahh-DNA1/DNA2-ahh-Rh there was a linear dependence on temperature, increasing from 3.3×10^{-13} cm^6 mmol^{-1} at 2 °C to 3.6×10^{-13} cm^6 mmol^{-1} at 85 °C. Our values are in agreement with previously reported values (*43*).

In the lower panel of Figure 5, the critical Förster distances, R_0 (eq 2), are shown, calculated assuming random relative orientation of the donor−acceptor pair ($\kappa^2 = {}^2/_3$).

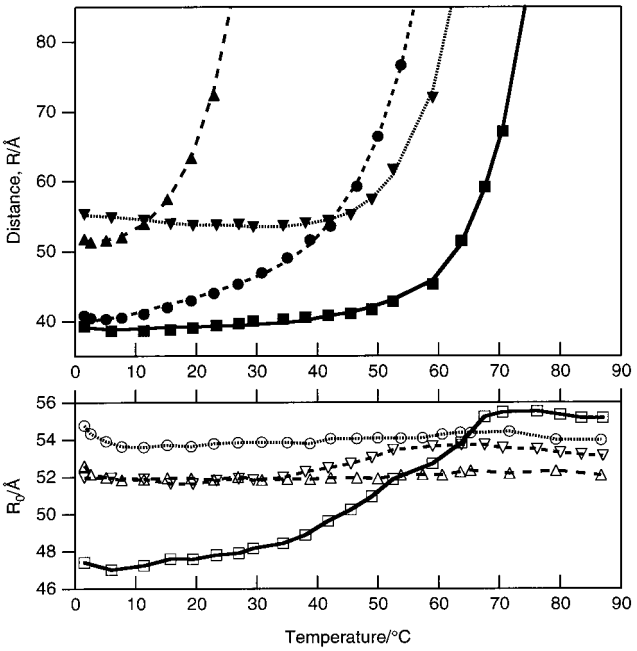

FIGURE 5: Donor−acceptor distance as calculated from fluorescence energy transfer. Top panel: (■) Fl-aha-PNA1/PNA2-aha-Rh, (▼) Fl-ahh-DNA1/PNA2-aha-Rh, (●) Fl-aha-PNA1/DNA2-ahh-Rh, and (▲) Fl-ahh-DNA1/DNA2-ahh-Rh. Bottom panel: critical Förster distance, R_0, of the Fl-Rh pair. (□) Fl and Rh on PNA, (▽) Fl on PNA and Rh on DNA, (○) Fl on DNA and Rh on PNA, and (△) Fl and Rh on DNA.

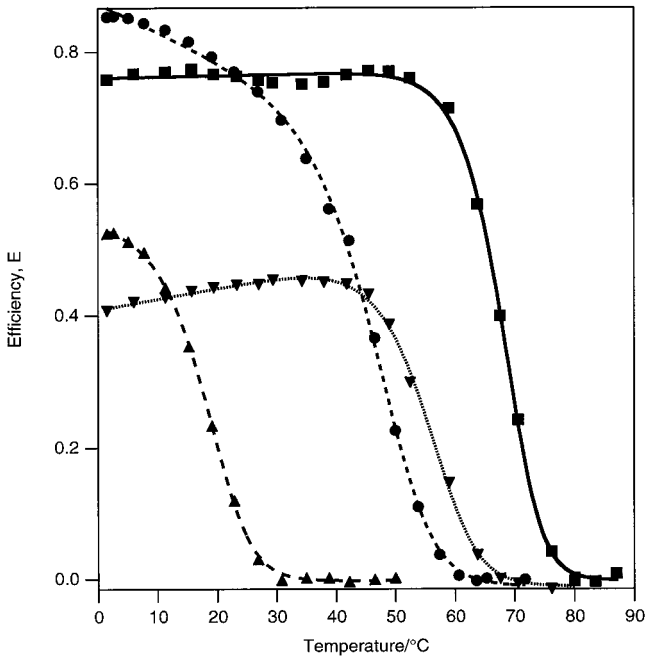

FIGURE 6: Energy transfer efficiency vs temperature. (■) Fl-aha-PNA1/PNA2-aha-Rh, (▼) Fl-ahh-DNA1/PNA2-aha-Rh, (●) Fl-aha-PNA1/DNA2-ahh-Rh, and (▲) Fl-ahh-DNA1/DNA2-ahh-Rh.

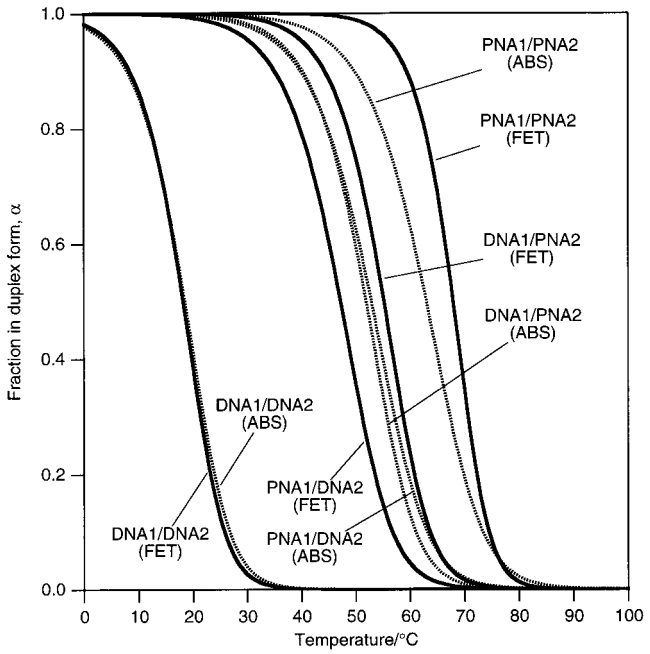

FIGURE 7: Fitted melting curves of the studied 10-mer PNA/PNA, PNA/DNA, and DNA/DNA duplexes, as obtained from absorbance hyperchromicity (ABS) and fluorescence energy transfer measurements (FET), respectively.

R_0 has been determined over the entire temperature range (1.5−87 °C), taking into account the temperature dependence of the spectral characteristics of fluorescein as noted previously (*22*). At 25 °C, the critical Förster distances are determined to be 48 Å for Fl-aha-PNA1/PNA2-aha-Rh, 52 Å for Fl-ahh-DNA1/PNA2-aha-Rh, 54 Å for Fl-aha-PNA1/DNA2-ahh-Rh, and 52 Å for Fl-ahh-DNA1/DNA2-ahh-Rh. In the literature, there are reports of Förster distances (assuming $\kappa^2 = {}^2/_3$) for the fluorescein−rhodamine pair between 49 and 54 Å at room temperature (*18, 44, 45*).

The anisotropies of fluorescein- and rhodamine-labeled double-stranded PNAs at 10 °C were around 0.12 for Fl and 0.14 for Rh, and were comparable to values obtained for fluorescein conjugated to oligonucleotides (*22, 24*). From the anisotropies, we estimate, using the protocols of Dale and co-workers (*29, 35*), that κ^2 is in the interval 0.4−1.9 at 25 °C. Hence, the standard assumption of κ^2 equal to ${}^2/_3$ at the lower temperatures may not be justified in this case. With κ^2 in the interval 0.4−1.9, a relatively large error level (−10/+20%) will be associated with the determined R_0 and the final interchromophoric distances in this case.

Energy Transfer. The fluorescence energy transfer efficiencies (*E*) of the samples Fl-aha-PNA1/PNA2-aha-Rh, Fl-ahh-DNA1/PNA2-aha-Rh, Fl-aha-PNA1/DNA2-ahh-Rh, and Fl-ahh-DNA1/PNA2-aha-Rh were measured at different temperatures as shown in Figure 6.

In the upper panel of Figure 5, the calculated interchromophoric distances for the four systems are shown. At low temperatures, i.e., when the strands are in duplex form, the distance between fluorescein and rhodamine is more or less constant and equal to 40 Å for Fl-aha-PNA1/PNA2-aha-Rh, 54 Å for Fl-ahh-DNA1/PNA2-aha-Rh, 44 Å for Fl-aha-PNA1/DNA2-ahh-Rh, and 51 Å for Fl-ahh-DNA1/DNA2-ahh-Rh. At the melting temperature, i.e., where half of the strands are dissociated, which occurs at 68 °C for PNA1/PNA2, at 47 °C for PNA1/DNA2, at 55 °C for DNA1/PNA2, and at 18 °C for DNA1/DNA2, the calculated distances increase rapidly.

Melting Curves. The energy transfer data (Figure 6) were converted to melting curves that show the fraction of strands in duplex form (α) vs temperature (Figure 7) by fitting the measured data to eqs 9 and 10 with the sloping base lines and $\Delta H°$ and T_m being fitting parameters, as described under Materials and Methods.

Table 1: Thermodynamic Parameters of the Formation of the Studied PNA/PNA, DNA/PNA, PNA/DNA, and DNA/DNA Duplexes from Single Strands, Obtained from Different Methods[a]

sample	T_m[b](°C)	$\Delta H°(T_m)$ (kJ/mol)	$T\Delta S°$(298 K) (kJ/mol)	$\Delta G°$(298 K) (kJ/mol)
	From Fluorescence Energy Transfer (FET) Experiments[c,d]			
Fl-aha-PNA1/PNA2-aha-Rh	68 (69)	-420 ± 19	-321 ± 15	-99 ± 34
Fl-ahh-DNA1/PNA2-aha-Rh	55 (57)	-303 ± 14	-232 ± 11	-71 ± 25
Fl-aha-PNA1/DNA2-ahh-Rh	47 (49)	-257 ± 14	-197 ± 11	-60 ± 25
Fl-ahh-DNA1/DNA1-ahh-Rh	18 (20)	-265 ± 16	-228 ± 14	-37 ± 30
	From Absorption Hyperchromicity (ABS) Experiments[c,e]			
PNA1/PNA2	63	-260 ± 7	-197 ± 6	-63 ± 13
DNA1/PNA2	52	-276 ± 8	-219 ± 7	-57 ± 15
PNA1/DNA2	53	-248 ± 8	-193 ± 7	-55 ± 15
DNA1/DNA2	18	-245 ± 8	-217 ± 7	-28 ± 15
	From Isothermal Titration Calorimetry (ITC) Experiments[e,f]			
PNA1/PNA2	–	-265 ± 11	-202 ± 24[g]	-63 ± 13[g]
DNA1/PNA2[h]	–	-212 ± 6	-162 ± 5	-50 ± 11
DNA1/DNA2[h]	–	-205 ± 4	-178 ± 4	-27 ± 8

[a] Measured in 10 mM phosphate buffer, pH 7.7. [b] Uncertainties in T_ms less than ±0.5 °C. [c] Errors in $\Delta H°$ and $T\Delta S°$ are standard deviations from the fitting procedure. [d] At 2.8 μM strand concentration. Values of T_m in parentheses correspond to 5 μM. [e] At 5 μM strand concentration. [f] Errors in $\Delta H°$ and $\Delta G°$ are taken as standard deviations from the fitting procedure. [g] The high equilibrium constant for PNA/PNA makes the titration curve steep at saturation and thus contains only a few data points giving problems fitting the binding constant (K). Therefore, we use the $\Delta G°$ from ABS measurements in this case to calculate $T\Delta S°$. [h] Measured at 10 °C, but $\Delta G°$ has been corrected to 298 K.

Figure 7 also shows fitted ordinary melting curves of three different complexes, from absorbance hyperchromicity measurements on the unlabeled decameric complexes PNA1/PNA2, DNA1/PNA2, PNA1/DNA2, and DNA1/DNA2. For all the studied duplexes, except for DNA1/DNA2, the melting curves determined with FET have sharper transitions compared to those determined with the standard absorption hyperchromicity technique. This difference is especially pronounced for the PNA/PNA duplexes, and, thus, for this duplex, the two techniques give distinctly different $\Delta H°$ values. As will be discussed below, this is attributed to interactions between the fluorescent dyes and the duplexes which give rise to an increased thermal stability of the labeled duplexes. The fitted thermodynamic parameters, T_m and $\Delta H°$, from analysis of the curves were used to calculate $T\Delta S°$. Combining $\Delta H°$ and $T\Delta S°$ yields $\Delta G°$. The calculated thermodynamic parameters are shown in Table 1.

As a complement to the FET and ABS measurements, we have also determined thermodynamic quantities of hybridization using isothermal titration calorimetry (ITC). The agreement between ABS and ITC thermodynamic parameters is reasonable at least for DNA/PNA and DNA/DNA duplexes. In the case of PNA/PNA, the ITC measurement gives only a reliable ΔH value, which agrees with that from absorption hyperchromicity, but due to the intrinsic problem of extracting both the ΔH and a high K value from the same titration, the $\Delta S°$ value is calculated from the ΔH from ITC and $\Delta G°$ from ABS. Consequently, the error in $\Delta S°$ will be larger. It should also be noted that the ITC values have been corrected for the pronounced self-melting (measured with ABS) of the single-stranded PNAs. This melting process is due either to dissociation of self-associated structures or to destacking of bases in the single strands. The correction is necessary since the ITC measurements are performed below the T_m of the single strands (about 40−45 °C). Unfortunately, the corrections introduce relatively large uncertainties in the final ITC values (for PNA-containing duplexes) due to the difficulty in evaluating the broad melting curves of the single strands. Therefore, we believe that of the methods used here, the ABS technique yields the most reliable thermodynamic information.

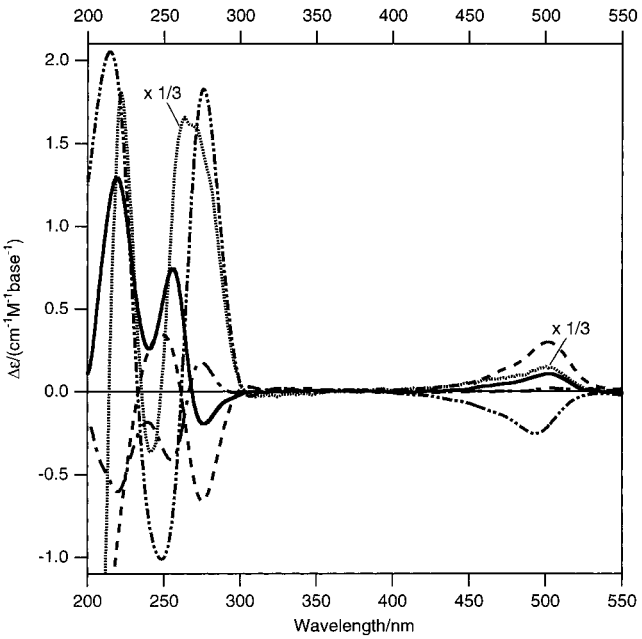

FIGURE 8: CD spectra of Fl-aha-PNA1/PNA2 (—), Fl-PNA1/PNA2 (— - —), Fl-aha-PNA1/DNA2 (— —), Fl-ahh-DNA1/PNA2 (•••, scaled by 1/3), and Fl-ahh-DNA1/DNA2 (— - - —).

Circular Dichroism Spectra. Figure 8 shows circular dichroism spectra of PNA/PNA duplexes with fluorescein attached either via a flexible linker or directly to the PNA, as well as the spectra of the Fl-ahh-DNA1/PNA2, Fl-ahh-DNA1/PNA2, and Fl-ahh-DNA1/DNA2 duplexes. Conjugation of fluorescein directly (no linker) to one of the ends (Fl-PNA1/PNA2) gives a spectrum very similar to that reported for the PNA1/PNA2 duplex (*9*). However, conjugation of the fluorescein label via the flexible aha-linker gives a radically different CD spectrum (Fl-aha-PNA1/PNA2), almost a perfect mirror image of that of unlabeled complex. In addition, an induced CD band appears in the fluorescein absorption region with a maximum at about 500 nm.

Upon increasing the temperature, the induced CD decreases (Figure 9). Also in the case of Fl-ahh-PNA1/DNA2, Fl-ahh-DNA1/PNA2, and Fl-ahh-DNA1/DNA2 we observe

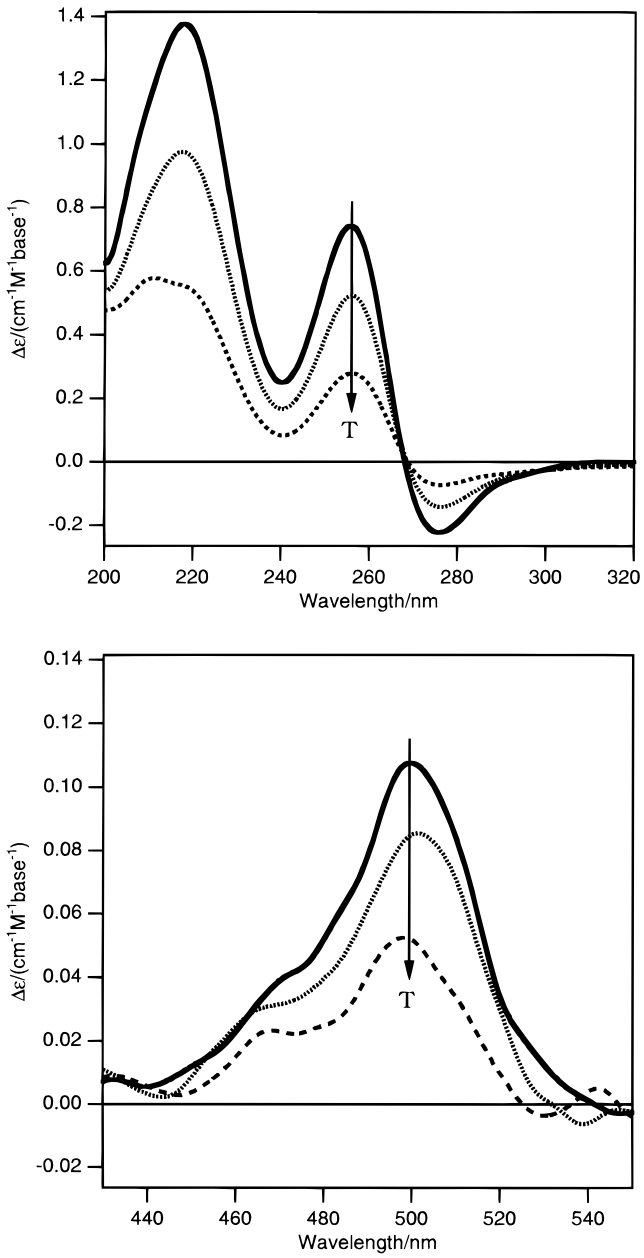

FIGURE 9: CD spectra of Fl-aha-PNA1/PNA2 at different temperatures (20, 35, and 50 °C).

induced CD in the absorption band of fluorescein, whereas in the 200−300 nm region the CD spectra are nearly identical to the spectra of the corresponding unlabeled duplex reported previously (*6*).

DISCUSSION

Thermodynamics of Hybridization. One of the objectives of this study was to characterize the hybridization thermodynamics of PNA/PNA and PNA/DNA duplexes and make comparison to the DNA/DNA duplex. At the low ionic strength conditions used, the lack of electrostatic charges in the PNA backbone is expected to be reflected in more favorable enthalpies of hybridization ($-\Delta H°$ larger) for the PNA1/PNA2, PNA1/DNA2, and DNA1/PNA2 duplexes compared with the DNA1/DNA2 duplex. This is indeed what is observed except for the PNA1/DNA2 duplex where the difference is very small and within the error margins of the ABS measurement. For this duplex, it is instead a more favorable entropic contribution that leads to the higher stability relative to the DNA1/DNA2 duplex.

For the three PNA-containing duplexes, the quotient $T\Delta S°/\Delta H°$ varies between 0.76 and 0.79 whereas for the DNA1/DNA2 duplex it equals 0.88. In a study of the ionic effects on the stability of 10-mer and 15-mer mixed-sequence PNA/PNA and PNA/DNA duplexes, it was found that these duplexes are destabilized by high concentrations (>1 M) of Na^+ salts with different monovalent anions (CH_3COO^-, Cl^-, and ClO_4^-) (*6*). The destabilizing effects followed the lyotropic series (*46*) with the least destabilization with CH_3COO^- and the largest destabilization with ClO_4^-. On the basis of these observations, it was suggested that hydrophobic interactions play an important role for the stabilization of PNA-containing duplexes. In addition, results from molecular-dynamics simulations suggest that the interaction of PNA with surrounding water molecules is much less favorable than the interaction of DNA with water (*11*). Thus, an interesting possibility is that the differences in water structure around the PNA and DNA backbones could explain our observation of more important enthalpic contributions to the free energy of hybridization for the PNA-containing duplexes. The importance of hydrophobic interactions for PNA/DNA hybridization will be further investigated in forthcoming studies. The relatively large entropic contribution in the case of the DNA/DNA complex is in agreement with the well-studied role of counterion association upon formation of this duplex (*47*, *48*).

Interestingly, the $\Delta H°$ and $T\Delta S°$ values for the PNA/PNA and PNA/DNA duplexes determined in this study are less negative than the values determined (with ABS) by Tomac et al. (*6*) for duplexes with the same sequence as used here but involving PNAs lacking L-lysines at the C-terminus. This indicates that the terminal lysine also plays a role in stabilizing the unlabeled duplexes. This is not surprising, since the positively charged lysine residue increases the solubility of PNA strands dramatically.

The different CD spectra and the different end-to-end distances obtained from FET measurements of the PNA1/DNA2 and DNA1/PNA2 duplexes indicate that these two duplexes have different structures. Thus, we expect different enthalpic and entropic contributions to the free energy of hybridization for these two duplexes. Indeed, we find small but significant differences in thermodynamic parameters for the mixed-sequence PNA1/DNA2 and DNA1/PNA2 duplexes, but the overall stability as reflected in T_m and $\Delta G°$ is nearly the same, probably due to enthalpy−entropy compensation (*49*). However, it must be noted that the thermal stability is certainly sequence-dependent, and the thermal stability range of PNA/DNA duplexes has been found to be larger than that seen for DNA/DNA duplexes. For instance, T_m of a PNA/DNA duplex varies from 35 °C for the PNA sequence TTTTCCTCTC (*50*) to 70 °C for the PNA sequence AAAAGGAGAG (*51*).

Fluorescein−PNA Interactions Change the Handedness of a PNA/PNA helix. The chirality of the terminal amino acid and choice of neighboring base pairs are known to influence the preferred helicity of PNA/PNA duplexes (*9*, *52*), but there is no simple relation to the absolute configuration of the amino acids (*52*). While the CD spectrum of the Fl-PNA1/PNA2 duplex is very similar to that of the

unlabeled duplex (Figure 8), the Fl-aha-PNA1/PNA2 complex has a CD spectrum in the 220−300 nm region which, in essence, is a mirror image of the PNA1/PNA2 spectrum with, however, about twice the molar CD amplitude. In addition, Fl-aha-PNA1/PNA2 displays a positive induced CD band corresponding to the fluorescein absorption band centered at 500 nm.

In a study of PNAs having 1−3 chiral cyclohexyl moieties inserted in the PNA backbone (*53*), it was concluded from correlation with melting temperature and CD data for the corresponding DNA/PNA duplexes that the PNA1/PNA2 duplex with L-lysine at the C-terminal is most probably a left-handed helix, which is opposite to the assignment in the first study by Wittung et al. (*9*). Since the CD spectrum of Fl-aha-PNA1/PNA2 in the 220−300 nm region is a mirror image of that of the PNA1/PNA2 duplex, we conclude that the fluorescein−aha attachment leads to a stabilization of the right-handed helix which becomes the dominating structure. A plausible mechanism behind this stabilization is a favorable electrostatic interaction between the dianionic fluorescein moiety and the dicationic chiral lysine on the opposite PNA strand. As the temperature is increased from 20 to 50 °C, which is still well below the melting temperature of the duplex, we observe a parallel decrease of the intensities of the 500 nm CD band and the CD bands between 220 and 300 nm (Figure 9). The decrease of the 500 nm band intensity with increasing temperature is direct evidence of a weakened interaction between the fluorescein and the PNA duplex. This, in turn, leads to a shift in equilibrium between right-handed and left-handed helices toward the left-handed one. Hence, the decrease of the CD signal in the 200−260 nm region is due to mutual cancellation by increasing amounts of the left-handed helices.

In the cases of Fl-aha-PNA1/DNA2, Fl-ahh-DNA1/PNA2, and Fl-ahh-DNA1/DNA2, we also observe induced CD bands around 500 nm (Figure 9). By contrast, in these cases, the CD spectra in the nucleobase region are very similar to those of the corresponding unlabeled duplexes which indicates that the helicity is preserved (*6*, *9*). The two mixed duplexes both have positive induced CD as in the case of the Fl-aha-PNA1/PNA2 duplex whereas the Fl-DNA1/DNA2 duplex exhibits negative induced CD. The difference in the sign of the induced CD could indicate a significantly different position of the fluorescein in the Fl-ahh-DNA1/DNA2 duplex compared with the other three duplexes studied.

To summarize, we have found that the equilibrium between left- and right-handed PNA1/PNA2 helices is strongly affected by the attachment of fluorescein via a flexible linker. This results in a net stabilization of the right-handed helix as evidenced from the reversal of sign of the CD spectrum. A similar reversal of sign has been observed by Wittung et al. for a PNA duplex with a terminal L-glutamic acid when changing the pH from 5 (neutral glutamate COOH group) to 7 (negatively charged COO^-) (*52*). Thus, it seems that it is quite easy to change the difference in free energy between the left- and right-handed helices and that it can be controlled by intrinsic (attached dyes) or extrinsic (pH, temperature) factors. This is not surprising since in the PNA/PNA duplex the effective mechanism of induction of chirality is thought to involve immobilization of rotation of the bonds near the amino acid (*52*). A slight perturbation of the environment around the terminal amino acid could then change the preferred helicity. For the 10-mer PNA/DNA and DNA/DNA duplexes, the preferred chirality is much more energetically favorable compared to that of the PNA/PNA duplex. This is so because each sugar−phosphate moiety provides a local bias contributing to the overall helicity.

Effects of the Fluorescent Labels on the Thermodynamics of Hybridization. The melting temperature (T_m) of a duplex is frequently used as a measure of the thermal stability. This is the temperature at which the fraction of single strands in duplex equals 50%.

According to the two-state model (*36*), T_m is expected to increase with concentration ($1/T_m$ is linearly dependent on $\ln c_T$). T_m values measured by the two techniques are expected to differ, since FET and ABS measurements are performed at different concentrations, due to different sensitivities of the two methods. Therefore, to compare the results of the two methods, the T_ms from the FET measurements were corrected for the difference in concentration (T_ms in parentheses in Table 1). Despite the correction, we see significant differences between the FET and ABS T_ms, ranging from a 4 °C lower FET than ABS T_m for the PNA1/DNA2 system up to a 6 °C higher T_m from FET for the PNA1/PNA2 system (Table 1).

The observed differences in thermodynamic parameters determined with the two methods can be due to either or both of the two following reasons: (1) The melting transitions cannot be described by a two-state (all-or-none) model; i.e., there is a significant population of intermediate states, which inherently lead to different melting curves from the two methods probing different physical properties. (2) The duplexes used in the FET measurements are stabilized/destabilized by the attached fluorescent dyes.

In the following, we argue that it is the second explanation, the influence from the dyes, that is the main cause for the observed discrepancies. Most importantly, we find the ABS T_ms of Fl-aha-PNA1/PNA2 (67 °C) and Fl-ahh-DNA1/PNA2 (55 °C) to be 3−4 °C higher than those of the corresponding unlabeled duplexes. This increase in T_m is comparable to the gain in stabilization, as judged from T_m, when an extra base pair is added to a PNA/DNA duplex (*54*).

Since the increase of 3−4 °C in T_m for the fluorescein-labeled PNA1/PNA2 and DNA1/PNA2 duplexes does not explain the whole difference between ABS and FET measurements on unlabeled and doubly labeled duplexes, respectively, the doubly labeled PNA1/PNA2 duplex was selected for further study using the ABS technique. The ABS T_m equals 70 °C, and the thermodynamic parameters ($\Delta H^\circ = -450$ kJ/mol and $T\Delta S^\circ = -344$ kJ/mol) of this duplex are found to have even more negative values than those from the FET measurements given in Table 1. Thus, it seems that the rhodamine labeling also can affect the hybridization thermodynamics.

The ABS T_m of Fl-aha-PNA1/DNA2 (41 °C) is 12 °C lower than that of the unlabeled duplex. In this case, the fluorescein conjugation leads to a significant destabilization probably originating from electrostatic repulsion between the dianionic fluorescein and the negatively charged DNA backbone. Addition of the rhodamine moiety to the DNA2 strand returns the T_m to that observed with FET (49 °C), but it is still lower than for the unlabeled PNA1/DNA2 duplex. The ABS T_m values of the Fl-ahh-DNA1/DNA2 (18 °C) and

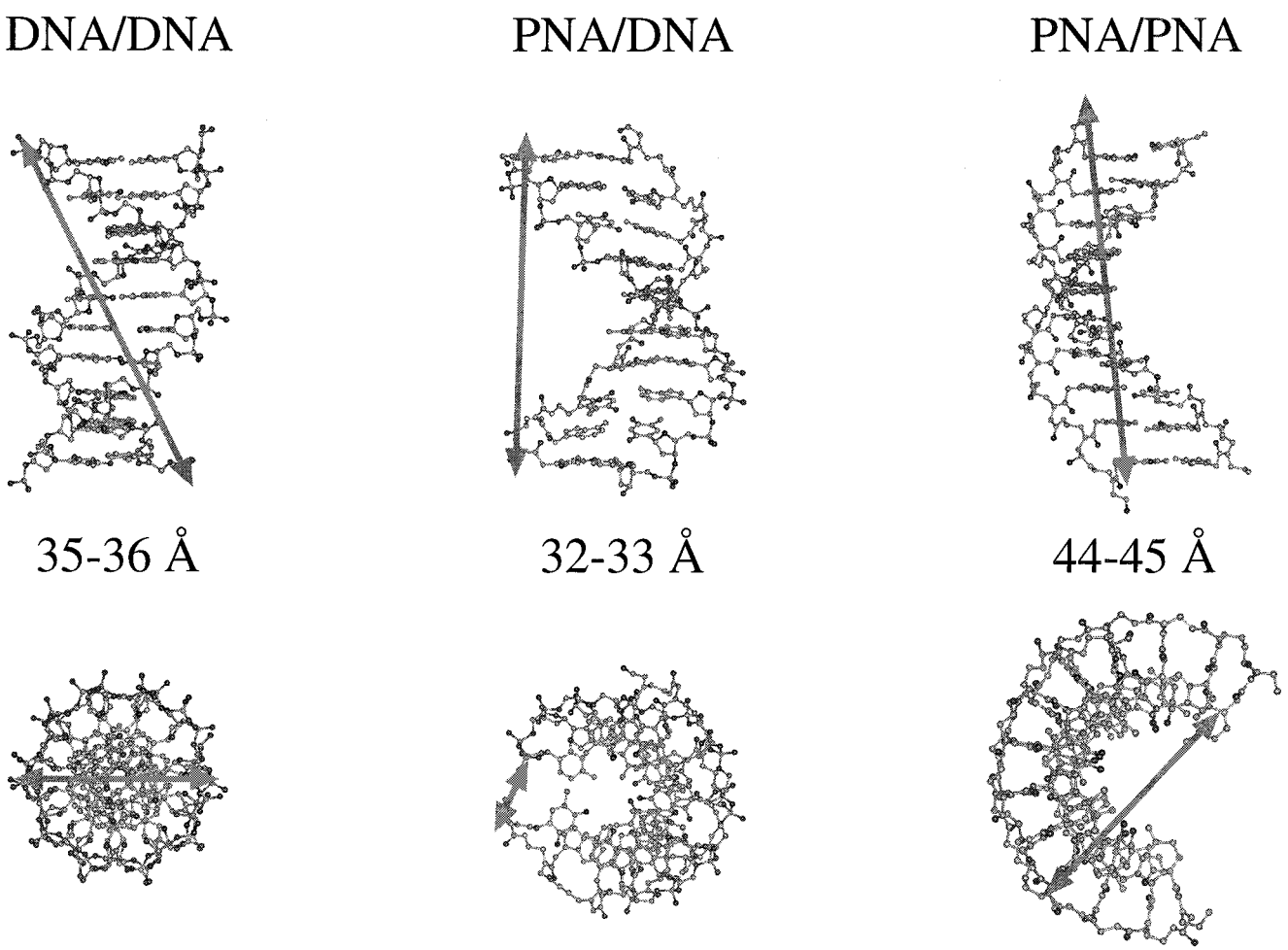

FIGURE 10: Models illustrating the three different types of duplexes. From left to right: DNA/DNA, PNA/DNA, and PNA/PNA, with side views in the upper row and top views in the lower. Arrows indicate distances between points of attachment of fluorescent labels and correspond to 35−36 Å (DNA/DNA), 32−33 Å (PNA/DNA), and 44−45 Å (PNA/PNA).

Fl-ahh-DNA1/DNA2-ahh-Rh duplexes (20 °C) are not significantly different from that of the unlabeled duplex (18 °C).

Thus, we conclude that the differences in thermodynamic parameters derived from the ABS and FET techniques are to a great extent due to dye/duplex interactions. This does not mean that the other potential origin (deviation from a two-state model) of a difference in results between the methods can be entirely excluded, although we have no evidence of additional, precursor complexes as was proposed in a previous kinetic study of PNA/DNA hybridization using the BIAcore technique (*55*).

One may envisage that the increased hydrophobicity of PNA and lack of electrostatic repulsion when a PNA strand is involved would increase the probability of formation of unspecific complexes. To test this idea, Fl-aha-PNA1 (Fl-aha-GTAGATCACT-Lys-NH_2) was mixed with a non-complementary 12-mer PNA labeled with rhodamine (H_2N-Lys-ATCAACACTGCA-Rh). PNA strands form duplexes preferentially in an antiparallel configuration, while the parallel configuration has a somewhat lower stability (*7*). The test Rh−PNA used has the potential to form several hydrogen-bonded base pairs antiparallel to the Fl-PNA; however, there would be either unpaired or bulging bases separating them, so a well-stacked duplex could never be formed. If some kind of non-base-paired outer-sphere complex, stabilized by hydrophobic interactions between the PNA backbones [as suggested by the crystal structure (*10*)], were formed, this species would have a reasonably strong energy transfer but little hypochromicity. No significant energy transfer was observed for this PNA/PNA pair which suggests that the formation of imperfect or outer-sphere complexes is not the cause of the observed differences between the FET and ABS results.

Structure of Duplexes. The average interchromophoric distances of the fully hybridized complexes obtained from FET measurements were 40 Å for the Fl-aha-PNA1/PNA2-aha-Rh duplex, 54 Å for the Fl-ahh-DNA1/PNA2-aha-Rh duplex, 44 Å for the Fl-aha-PNA1/DNA2-ahh-Rh, and 51 Å for Fl-ahh-DNA1/PNA2-ahh-Rh. These distances can be compared to the maximum distances, obtained from simple molecular modeling (Figure 10).

The decameric DNA/DNA duplex was modeled as a standard B-form structure. In this case, the fluorophores are attached not only to different ends, but also on opposite strands of the helix which leads to a distance of 35−36 Å between the points of attachment. A PNA/DNA decamer was constructed correspondingly, by extending the solution NMR structure of a PNA/DNA octamer (*56*). The end-to-end distance was then estimated to be 32−33 Å. In the case of the PNA/PNA duplex, the corresponding distance is estimated to be 44−45 Å on the basis of the crystal structure

of a PNA/PNA hexamer (*10*).

Assuming fully extended linker arms, the maximum distances between the dyes for the labeled PNA1/PNA2, PNA1/DNA2, and DNA1/DNA2 duplexes are estimated to be 75, 63, and 65 Å, respectively. However, since the linker arms are flexible, we expect shorter distances, and bearing in mind the indications of interaction between dyes and duplexes observed in the CD, anisotropy, and thermodynamic measurements, the shorter measured distance is a strong indication that the stack of bases in all duplexes studied is elongated. This is in agreement with the relatively extended solution NMR structure of a PNA/DNA octamer and adds support to that the crystal structure of the PNA/PNA hexamer is also relevant in solution.

CONCLUSIONS

(1) The hybridization thermodynamics for the formation of mixed sequence decamer DNA/DNA, DNA/PNA, and PNA/PNA duplexes have been characterized using fluorescence energy transfer (FET), absorption hypochromicity (ABS), circular dichroism (CD), and isothermal titration calorimetry (ITC). Overall, the methods give consistent values of enthalpy and entropy of hybridization, but interactions of fluorescent probes affect the results. We see no indications of outer-sphere precursor complexes, and the hybridization can be perfectly described by a two-state model.

(2) The end-to-end distances obtained for the decameric PNA/DNA and PNA/PNA duplexes in solution are all found to agree well with structures determined by NMR (*56*) and X-ray crystallographic (*10*) techniques, indicating that extended conformations are adopted also in solution.

(3) Fluorescein conjugated via a flexible linker to one of the strands in the PNA1/PNA2 duplex stabilizes the right-handed helical form, probably via an electrostatic interaction between the fluorescein and the adjacent lysine on the opposite PNA strand. The stabilization leads to a shift of the equilibrium toward an excess of the right-handed helix.

(4) The fluorescence properties of the dyes, especially those conjugated to PNAs, are highly temperature dependent, and the temperature dependence has to be determined if FET experiments are used for quantitative purposes.

REFERENCES

1. Nielsen, P. E. (1991) *Bioconjugate Chem. 2*, 1−12.
2. Uhlmann, E., and Peyman, A. (1990) *Chem. Rev. 90*, 543−584.
3. Nielsen, P. E., Egholm, M., Berg, R. H., and Buchardt, O. (1991) *Science 254*, 1497−1500.
4. Egholm, M., Buchardt, O., Nielsen, P. E., and Berg, R. H. (1992) *J. Am. Chem. Soc. 114*, 1895−1897.
5. Egholm, M., Nielsen, P. E., Buchard, O., and Berg, R. H. (1992) *J. Am. Chem. Soc. 114*, 9677−9678.
6. Tomac, S., Sarkar, M., Ratilainen, T., Wittung, P., Nielsen, P. E., Nordén, B., and Gräslund, A. (1996) *J. Am. Chem. Soc. 118*, 5544−5552.
7. Eriksson, M., and Nielsen, P. E. (1996) *Q. Rev. Biophys. 29*, 369−394.
8. Kim, S. K., Nielsen, P. E., Egholm, M., Buchardt, O., Berg, R. H., and Nordén, B. (1993) *J. Am. Chem. Soc. 115*, 6477−6481.
9. Wittung, P., Nielsen, P. E., Buchardt, O., Egholm, M., and Nordén, B. (1994) *Nature 368*, 561−563.
10. Rasmussen, H., Kastrup, J. S., Nielsen, J. N., Nielsen, J. M., and Nielsen, P. E. (1997) *Nat. Struct. Biol. 4*, 98−101.
11. Sen, S., and Nilsson, L. (1998) *J. Am. Chem. Soc. 120*, 619−631.
12. Knudsen, H., and Nielsen, P. E. (1996) *Nucleic Acids Res. 24*, 494−500.
13. Hanvey, J. C., Peffer, N. J., Bisi, J. E., Thomson, S. A., Cadilla, R., Josey, J. A., Ricca, D. J., Hassman, F., Bonham, M. A., Au, K. G., Carter, S. G., Bruckenstein, D. A., Boyd, A. L., Noble, S. A., and Babiss, L. E. (1992) *Science 258*, 1481−1485.
14. Møllegaard, N. E., Buchardt, O., Egholm, M., and Nielsen, P. E. (1994) *Proc. Natl. Acad. Sci. U.S.A. 91*, 3892−3895.
15. Nielsen, P. E., Egholm, M., Berg, R. H., and Buchardt, O. (1993) *Nucleic Acids Res. 21*, 197−200.
16. Carlsson, C., Jonsson, M., Nordén, B., Dulay, M. T., Zare, R. N., Noolandi, J., Nielsen, P. E., Tsui, L.-Z., and Zielenski, J. (1996) *Nature 380*, 207.
17. Ørum, H., Nielsen, P. E., Egholm, M., Berg, R. H., Buchardt, O., and Stanley, C. (1993) *Nucleic Acids Res. 21*, 5332−5336.
18. Cardullo, R. A., Agrawal, S., Flores, C., Wolf, D. E., and Zamecnik, P. C. (1988) *Proc. Natl. Acad. Sci. U.S.A. 85*, 8790−8794.
19. Murakami, A., Nakaura, M., Nakatsuji, Y., Nagahara, S., Tran-Cong, Q., and Makino, K. (1991) *Nucleic Acids Res. 19*, 4097−4102.
20. Morrison, L. E., and Stols, L. M. (1993) *Biochemistry 32*, 3095−3104.
21. Murchie, A. I. H., Lilley, D. M. J., Clegg, R. M., Duckett, D. R., Diekmann, S., and Vonkitzing, E. (1989) *Nature 341*, 763−766.
22. Clegg, R. M., Murchie, A. I. H., Zechel, A., and Lilley, D. M. J. (1993) *Proc. Natl. Acad. Sci. U.S.A. 90*, 2994−2998.
23. Christensen, L., Fitzpatrick, R., Gildea, B., Petersen, K. H., Hansen, H. F., Koch, T., Egholm, M., Buchardt, O., Nielsen, P. E., Coull, J., and Berg, R. H. (1995) *J. Pept. Sci. 3*, 175−183.
24. Dawson, R. M. C., Elliott, D. C., Elliott, W. H., and Jones, K. M. (1986) in *Data for biochemical research*, pp 103−114,, Oxford University Press, New York.
25. Haugland, R. P. (1994) *Handbook of fluorescent probes and research chemicals*, 5th ed., Molecular Probes, Inc., Eugene.
26. Förster, T. (1948) *Ann. Phys. 2*, 55−75.
27. Förster, T. (1949) *Z. Naturforsch. 4A*, 321−327.
28. Förster, T. (1959) *Discuss. Faraday Soc. 27*, 7−17.
29. Dale, R. E., and Eisinger, J. (1975) in *Biochemical Fluorescence: Concepts* (Chen, F., and Edelhoch, H., Eds.) pp 115−284, Marcel Dekker, Inc., New York.
30. Clegg, R. M. (1992) *Methods Enzymol. 211*, 353−388.
31. Nordén, B., Kubista, M., and Kurucsev, T. (1992) *Q. Rev. Biophys. 25*, 51−170.
32. Lakowicz, J. R. (1983) *Principles of fluorescence spectroscopy*, Plenum Press, New York.
33. Kubista, M., Sjöback, R., Eriksson, S., and Albinsson, B. (1994) *Analyst 119*, 417−419.
34. Weber, G., and Teale, F. W. J. (1957) *Trans. Faraday Soc. 53*, 646−655.
35. Dale, R. E., Eisinger, J., and Blumberg, W. E. (1979) *Biophys. J. 26*, 161−194.
36. Applequist, J., and Damle, V. (1965) *J. Am. Chem. Soc. 87*, 1450−1458.
37. Puglisi, J. D., and Tinoco, J. I. (1989) *Methods Enzymol. 180*, 304−325.
38. Marky, L. A., and Breslauer, K. J. (1987) *Biopolymers 26*, 1601−1620.
39. Draper, D. E., and Gluick, T. C. (1995) *Methods Enzymol. 259*, 281−351.
40. Mergny, J. L., Boutorine, A. S., Garestier, T., Belloc, F., Rougée, M., Bulychev, N. V., Koshkin, A. A., Bourson, J., Lebedev, A. V., Valeur, B., Thuong, N. T., and Hélène, C. (1994) *Nucleic Acids Res. 22*, 920−928.
41. Fairclough, R. H., and Cantor, C. R. (1978) *Methods Enzymol. 48*, 347−379.

42. Cooper, J. P., and Hagerman, P. J. (1990) *Biochemistry 29*, 9261−9268.
43. Furey, W. S., Joyce, C. M., Osborne, M. A., Klenerman, D., Peliska, J. A., and Balasubramanian, S. (1998) *Biochemistry 37*, 2979−2990.
44. Holowka, D., and Baird, B. (1983) *Biochemistry 22*, 3466−3474.
45. Wu, P., and Brand, L. (1994) *Anal. Biochem. 218*, 1−13.
46. Collins, K. D., and Washabaugh, M. W. (1985) *Q. Rev. Biophys. 18*, 323−422.
47. Record, M. T., Jr., Anderson, C. F., and Lohman, T. M. (1978) *Q. Rev. Biophys. 11*, 103−178.
48. Manning, G. S. (1978) *Q. Rev. Biophys. 11*, 179−246.
49. Searle, M. S., and Williams, D. H. (1993) *Nucleic Acids Res. 21*, 2051−2056.
50. Nielsen, P. E. (unpublished results).
51. Nielsen, P. E., and Christensen, L. (1996) *J. Am. Chem. Soc. 118*, 2287−2288.
52. Wittung, P., Eriksson, M., Lyng, R., Nielsen, P. E., and Nordén, B. (1995) *J. Am. Chem. Soc. 117*, 10167−10173.
53. Lagriffoule, P., Wittung, P., Eriksson, M., Kilså Jensen, K., Nordén, B., Buchardt, O., and Nielsen, P. E. (1997) *Chem. Eur. J. 3*, 912−919.
54. Ratilainen, T., Holmén, A., Tuite, E., Nielsen, P., and Nordén, B. (unpublished results).
55. Kilså Jensen, K., Ørum, H., Nielsen, P. E., and Nordén, B. (1997) *Biochemistry 36*, 5072−5077.
56. Eriksson, M., and Nielsen, P. (1996) *Nat. Struct. Biol. 3*, 410−413.

BI9808722